remote sensing

MDPI

Article

Satellite-Based Mapping of Gold-Mining-Related Land-Cover Changes in the Magadan Region, Northeast Russia

Andrey Shikhov [1,2,*], Polina Ilyushina [1,3], Olga Makarieva [1,4], Anastasiia Zemlianskova [1,4] and Maria Mozgina [2]

[1] Earth Science Institute, St. Petersburg State University, 199034 St. Petersburg, Russia; polinam_20@mail.ru (P.I.); o.makareva@spbu.ru (O.M.)
[2] Faculty of Geography, Perm State University, 614990 Perm, Russia
[3] Faculty of Geography, M.V. Lomonosov Moscow State University, 119991 Moscow, Russia
[4] Department of Monitoring and Forecasting Climate Change and the Environment, North-Eastern State University, 685000 Magadan, Russia
* Correspondence: a.shikhov@spbu.ru or shikhovan@gmail.com; Tel.: +7-951-937-00-63

Abstract: Gold mining generates major environmental impacts like landscape degradation, accumulation of waste rock dumps, and water contamination by suspended solids. Russia ranks third in the world in gold production, but the impact of gold mining has not been previously estimated for its vast northeastern part. This study provides a detailed overview of land-cover changes associated with gold mining in the Magadan region (northeast Russia) in the 21st century, where alluvial gold production has increased by a third in the last 20 years. A long-term series of Landsat and Sentinel-2 images obtained in July and August are used to compile two datasets of mining-impacted areas with totally removed vegetation for 2000–2002 and 2022. We calculated the NDVI difference and then discriminated mining-related vegetation losses from other bare areas, using additional data like the classification of landforms based on the digital surface model and the data on mining allotments. The total area of gold-mining sites was estimated as 41,206 ha in 2000–2002 and 72,602 ha in 2022, with an increase of 26,031 ha over the past 4–6 years. Moreover, this is a lower-boundary estimate, without taking into account man-made reservoirs and historical mines recovered by vegetation. The spatial distribution of mining sites has not changed significantly over the past two decades and has a maximum in the western part of the region. We found that the floodplains of the Berelekh and Debin Rivers (large tributaries of the Kolyma River) are most heavily impacted by gold mining with a removed vegetation canopy occupying 16.0% and 11.2% of their area. Along with the land degradation assessment, we found that 19,900 ha of historical gold-mining sites in the Berelekh River basin are recovered by vegetation, which is comparable in size to the areas impacted by mining over the past 20 years.

Keywords: gold mining; land degradation; Landsat and Sentinel-2 images; NDVI; landforms classification; Google Earth Engine; vegetation recovery; Magadan region

Citation: Shikhov, A.; Ilyushina, P.; Makarieva, O.; Zemlianskova, A.; Mozgina, M. Satellite-Based Mapping of Gold-Mining-Related Land-Cover Changes in the Magadan Region, Northeast Russia. *Remote Sens.* **2023**, *15*, 3564. https://doi.org/10.3390/rs15143564

Academic Editors: Izaya Numata and Deodato Tapete

Received: 31 May 2023
Revised: 29 June 2023
Accepted: 14 July 2023
Published: 16 July 2023

1. Introduction

Mining is one of the most important drivers of landscape transformation. Estimates suggest that mining and quarrying activities have modified roughly 0.3–0.8 Mkm^2 of land around the world, and this trend is continuing [1]. Gold mining, like other mining industries, can cause a wide range of adverse impacts during mining operations and after closure [2]. In particular, the first step of gold mining from ore deposits is an excavation of a large amount of geological material, which is disposed of on land in the form of waste rock dumps. Then, the ore is processed by crushing/grinding, gravity separation, and chemical extraction of the gold. During gold extraction, large amounts of materials with potentially hazardous chemical properties are produced and disposed of as tailing storage facilities (TSFs), slime dams, or tailing dams [3,4]. On the other hand, mining in alluvial placers usually aims to extract gold from stream sediments and floodplains using bulldozers,

dredges, and hydraulic jets of water (a process called "hydraulic mining"). Because placer mining is often carried out in a streambed, it is an environmentally destructive type of mining, releasing large quantities of sediment that can impact surface water for dozens of kilometers downstream of the placer mine [5].

Gold mining in alluvial placers is accompanied by soil and vegetation destruction, landscape fragmentation, and biodiversity loss, and interrupts ecosystem service flows [6,7]. It presents a substantial driver of deforestation, unique in its severity of impacts and leaving a highly altered landscape [8–10]. Gold mining's impact on river systems results in the disturbance of riverbeds, water contamination with suspended solids, and toxic heavy metals that are leached from tailings [5,6,11–14]. According to the database presented by the authors in [15], the number of gold mines is substantially greater than the number of mines of any other commodity.

Gold-mining impacts on the environment, like water pollution and land degradation, are well-detected by remote sensing tools and techniques. Therefore, its use provides substantial benefits for the detection, mapping, and monitoring of gold-mining activities and their effects, especially associated with placer mining [16]. Satellite and aerial images are mostly applied to monitor three major variables in the gold-mining context, namely deforestation or land-cover change [8–10,17], water pollution caused by mining activity in proximity to rivers or on river channels by detecting water turbidity levels in stream channels [18,19], and mercury presence estimation [20]. Satellite images with medium (Landsat, Sentinel-2) and high (SPOT-6, Worldview-2, etc.) spatial resolution have been used to identify mining activity and impact [17,21]. Optical images are analyzed using diverse approaches like image classification [7,22], spectral indices [23,24], time series analysis [18], and various machine-learning algorithms like random forest and convolutional neural networks [21,25,26]. Water contamination by gold mining is remotely estimated through total suspended matter (TSM), which is a proxy of water turbidity (the most widespread contamination associated with gold mining). TSM is calculated from both multispectral [27] and hyperspectral [28] satellite images. Where atmospheric conditions (e.g., cloud cover and seasonal burning) prevent the use of optical images to observe gold-mining areas, the time series of radar data (mainly Sentinel-1) are successfully applied to identify land-cover changes [29,30].

Along with satellite images, gold-mining monitoring at all stages of development (from exploration to reclamation) is carried out with traditional aerial imagery [31] and unmanned aerial vehicles (UAVs) [32]. Compared to other monitoring methods, UAVs provide a short revisit period and fast data acquisition, as well as simple operations [33]. Multispectral and hyperspectral images from UAVs are inputs for land-cover classification at a local scale [34], acid mine drainage detection [35], and other applications in gold-mining regions [33].

Presently, Russia leads the world in terms of area occupied by mining land use (at least 11,770 km^2) [14]. A substantial part of the total impacted area is related to gold mining in alluvial placers in Central Siberia and the Far East. However, land degradation related to gold mining has been inventoried only fragmentarily, for example [36]. In northeastern Russia, the extent and dynamics of mining-related land degradation remain unknown.

The environmental impact of gold mining is especially large-scale in the Magadan region, located in northeastern Russia, in a subarctic extra-continental climate and continuous permafrost zone. The Magadan region is the leader in terms of alluvial gold production in Russia, where gold mining has been intensively developing for over 80 years [37]. The total alluvial gold production here increased from 14.5 tons in 2013 to 19.65 tons in 2022. About 20 ore deposits and 300 alluvial placers are being exploited to date [38]. The area impacted by gold mining was preliminarily estimated as 2% of the total area of Susuman, Ten'kinsky, and Yagodninsky municipal districts in the western part of the Magadan region [39].

Placer mining in permafrost areas can lead to much more significant changes in the environment in comparison to non-permafrost areas. The extraction of sediment disrupts the insulating layer of vegetation and soil above the permafrost. Climate warming acceler-

ates permafrost degradation following surface disturbance [40]. Thawing permafrost may result in hazardous geocryological processes like thermokarst, thermal erosion, solifluction, pingos, ground subsidence, and instability [41,42], also altering the hydrological regime through increased erosion and sedimentation. The restoration of impacted landscapes in cold climates and permafrost landscapes takes a long time [43].

In this study, we present the first assessment of the extent of land degradation caused by gold mining in the Magadan region and its changes in the 21st century based on Landsat/Sentinel-2 satellite data. Along with land degradation, we estimate vegetation recovery on lands impacted in previous years.

2. Materials and Methods

2.1. Study Region

The Magadan region stretches across the northeastern part of Russia, bordered by the Sea of Okhotsk to the east and the Chukotka Autonomous Okrug to the northeast. It is situated within the larger Russian Far East, which encompasses vast territories of eastern Russia. The region spans approximately 462,000 km^2. The Magadan region experiences a subarctic climate, characterized by long, cold winters and relatively short, cool summers. The region's climate is heavily influenced by its coastal location and proximity to the Sea of Okhotsk. The landscape of the Magadan region is diverse. It is dominated by mountain ranges, including the Kolyma Range and the Verkhoyansk Range, which are part of the larger East Siberian System. These mountains are characterized by rugged peaks, deep valleys, and numerous rivers that cut through the terrain. The region is also home to vast stretches of tundra, a treeless biome found in high latitudes. Inland, the region is dotted with numerous rivers, including the Kolyma River, one of the largest rivers in northeastern Russia. More than 98% of the territory of the Magadan region is in the permafrost zone, which mostly has a continuous distribution. The Magadan region is rich in mineral resources. It ranks first and second in Russia in terms of alluvial gold production and the scale of predicted resources of bedrock gold, respectively [44]. The most promising gold mines, like the Pavlik, Natalka, and Degdekan deposits, are in the western part of the region, in the Ten'kinsky and Susumansky districts (Figure 1).

2.2. Compilation of GIS Datasets of Mining-Related Land Degradation

2.2.1. Initial Data

We used freely available data from Landsat and Sentinel-2 satellites to delineate the gold-mining sites (without classification into ore and alluvial deposits) in the Magadan region, and various additional data to distinguish from the areas with spectral characteristics similar to them (Table 1). As noted in previous studies [45], satellite images with a spatial resolution of 30 m have been available for the territory of the Magadan region only since 1999, when the Landsat-7 satellite with the ETM+ sensor was launched. Earlier data from the Landsat-1 satellite (MSS sensor) are available for 1973−1975; however, the spatial resolution is insufficient to correctly delineate gold-mining sites (except for the largest areas), and the images for the growing season (July–August) do not cover the entire region. Therefore, we consider land degradation only for the period 1999−2022.

It is well known that placer gold-mining leads to the total removal of soil and vegetation canopy, which is accompanied by a substantial decrease in the Normalized Difference Vegetation Index (NDVI) [22,23,25]. However, in the subarctic climate of the Magadan region with a short growing season [46], vegetation loss can only be identified from summertime images, obtained from late June to August or early September. Substantial cloudiness also challenges the selection of appropriate images, especially for the period 2003−2012, when mainly Landsat-7 images after scan line corrector failure (SLC-off) are available [47]. Only after the launch of the Landsat-8 satellite in 2013, and Sentinel 2A/2B satellites in 2015 and 2017, did the frequency of obtaining cloud-free images become sufficient for the annual monitoring of land degradation.

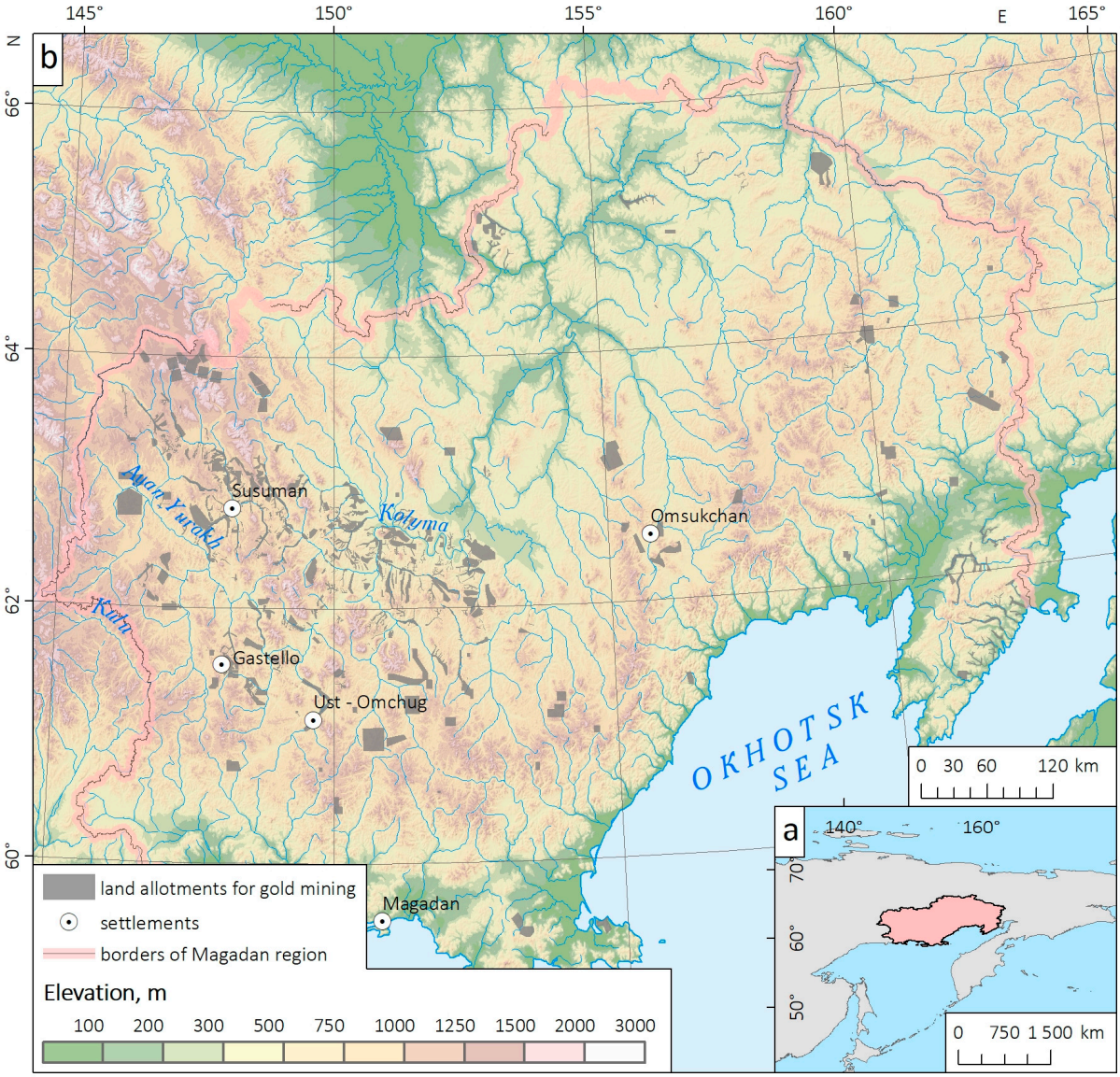

Figure 1. Geolocation of the Magadan region (**a**), and its base map (**b**). Land allotments for gold mining are also shown.

Due to the above-mentioned data limitations, three continuous coverages of cloudless summertime images were collected for the Magadan region, namely Landsat-7 for 2000−2002, and Sentinel-2 for 2016−2018 and 2022 (Table 1). Taking into account the subsequent calculation of NDVI, sensitive to atmospheric effects, we downloaded Landsat Collection 2 Level 2 surface reflectance data, generated using the Landsat Ecosystem Disturbance Adaptive Processing System (LEDAPS) algorithm (version 3.4.0) [48]. In total, we used 16 Landsat-7 ETM+ images for 2000−2002, with imagery dates ranging from 9 July to 17 August and cloud cover less than 10%. These images completely cover the Magadan region, except for the areas unaffected by gold mining (Figure 1). Two other data coverages consist of Sentinel-2 images of Level2A processing level, generated using the Sen2Cor atmospheric correction algorithm [49]. Pairs of Sentinel-2 images were obtained for 26 tiles of the Sentinel-2 Tiling Grid. Imagery dates range from 26 June to 31 August, and cloud cover is less than 10%. Landsat images were downloaded from USGS EarthExplorer [50], and Sentinel-2 images from EOS LandViewer [51].

Various natural surfaces like alluvial deposits, aufeis glades, mountainous rocky landscapes (so-called "*goltsy*"), as well as several fire scars, have close-to-zero values of

NDVI and other spectral characteristics similar to degraded lands. Therefore, we used various additional data to discriminate mining sites from other land-cover/land-use types. It is of note that there is no universal signature to discriminate them from mining areas. Thus, alluvial gold mining is concentrated in stream valleys, and we used a digital surface model (DSM) ALOS World Topographic Data [52] (Table 1) to identify streams and valleys. By contrast, gold mining in ore deposits is not associated with river valleys, and we used the data on mining allotments to identify these areas. Thus, we analyzed both features based on DSM and the data on mining allotments and used high-resolution satellite images from open map services for visual inspection (see Sections 2.2.3 and 2.2.4 for details).

Table 1. Overview of the data used to delineate the gold-mining areas.

Data Type	Data Source	Spatial Resolution	Time Period	Work Stage
Satellite images	Landsat-7 ETM+ and Landsat-5 TM	30 m	2000–2002 2003–2012	Delineation of lands impacted by gold mining over 20 years ago Identification of land-cover changes and vegetation recovery on mining areas
	Landsat-8 OLI	30 m	2013–2022	
	Sentinel-2 images	10 m	2016–2018 and 2022	Assessment of the actual area of impacted lands and its changes between 2016–2018 and 2022
	High-resolution satellite images from open map services (Google Earth, Bing Maps, ESRI)	≈0.5 m	All available images (2009—present)	Visual inspection of selected mining sites
Additional data	ALOS WTD digital surface model	30 m	–	Identification of thalwegs, terrain classification, delineation of river basins
	Land allotments for gold mining	–	2021	Separation of mining areas from other spectrally similar surfaces
	NASA active fire data [53]	700/1000 m	2000–2022	Discrimination of mining areas from fire scars
	Land-cover/land-use maps GlobCover-2009 [54], and the map of vegetation cover of Russia [55]	230 m	2018	Determination of vegetation cover types impacted by gold mining

2.2.2. Spectral Characteristics of Mining Sites and Natural Bare Areas

As noted above, land impacted by gold mining has similar spectral characteristics to natural bare areas. We compared the spectra based on Sentinel-2 images (L2A processing level), obtained in mid-summer of 2022. Several mining sites, as well as natural alluvial deposits, mountainous rocky wastelands, and burned areas, were selected to calculate their spectral characteristics (test areas included several hundred pixels for each class). Then, spectral reflectance was averaged for them (Figure 2). All these classes have close-to-zero NDVI values. Spectral characteristics of natural alluvial deposits almost do not differ from the same of mining areas, while mountainous rocky landscapes and especially burned areas have, on average, lower reflectance in visible and near-infrared bands, and higher reflectance in shortwave and mid-infrared bands. However, maximum and minimum values of spectral reflectance for mining sites, fire scars, and mountainous rocky landscapes overlap, which indicates a substantial likelihood of confusion between these classes [56]. This indicates the need to use the above-mentioned additional information (Table 1) to identify gold-mining areas from satellite images.

2.2.3. Identification of Mining Sites from Landsat Images for 2000–2002

Historical gold-mining areas (for 2000−2002) are identified based on 16 Landsat-7 ETM+ scenes obtained in July and August. Identification is performed as a two-stage procedure. In the first stage, we detected all the bare areas, and in the second stage, we selected among them the areas impacted by gold mining. The geoprocessing model was compiled in ArcGIS ModelBuilder to execute the workflow.

NDVI was calculated as (B5 − B4)/(B5 + B4), where B5 and B4 are near-infrared and red bands of Landsat 7 ETM+ images, respectively. Threshold values of NDVI are used

to identify bare areas. We found that typical values of NDVI for gold-mining areas with totally removed vegetation range from −0.05 to 0.1 (Figure 3b).

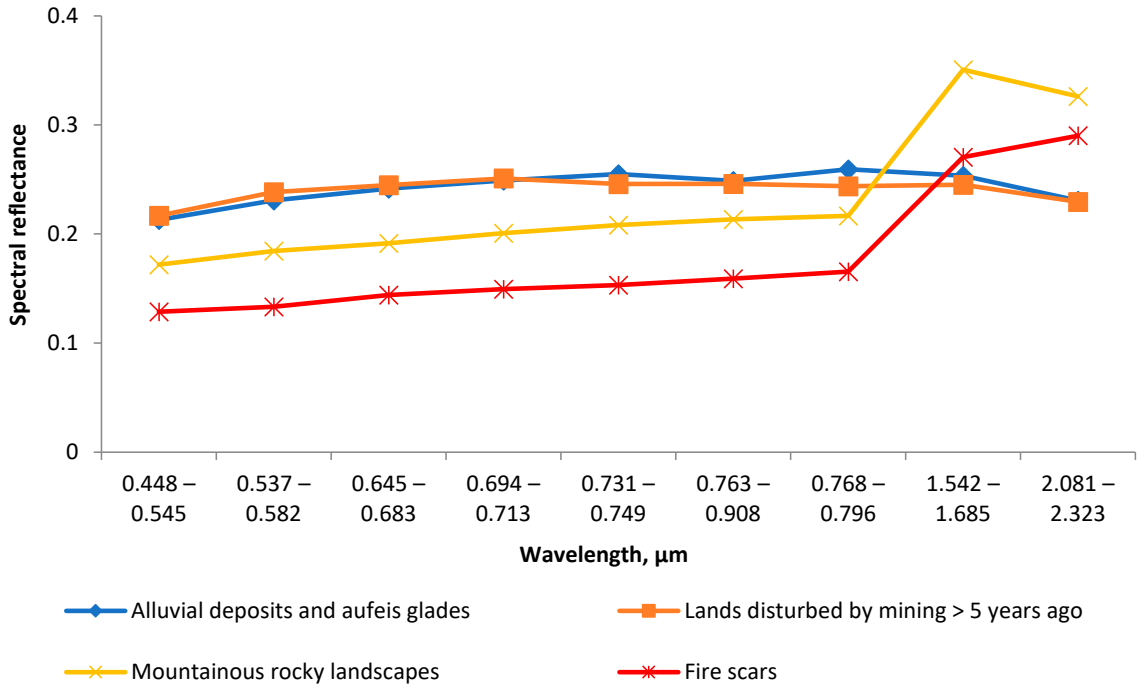

Figure 2. Spectra of land impacted by gold mining compared with other types of bare areas.

Land/water masking is performed using the Modified Normalized Difference Water Index mNDVI [57], calculated as (B3 − B6)/(B3 + B6), where B3 and B6 are green and shortwave infrared bands of Landsat 7 ETM+ images, respectively. Water bodies (including man-made dams and reservoirs in mining-impacted floodplains) are masked by a threshold value of mNDVI, which was taken equal to 0.25. Threshold values of both NDVI and mNDWI have been verified for several Landsat images and then used to identify bare areas. Historical mining sites with recovering vegetation are not detected using such an NDVI threshold.

In the second stage, we used additional data to discriminate mining areas from other bare areas. First, alluvial gold mining is concentrated in river valleys. Therefore, we used the ALOS WTD digital surface model to identify stream networks (with ArcGIS Spatial Analyst tools) and perform TPI-based landform classification [58] with SAGA GIS (System for Automated Geoscientific Analysis). Bare areas that intersected with five landform classes, namely "Mountain Tops and High Ridges", "Midslope Ridges and Small Hills in Plains", "Local Ridges, Hills in Local Ridges, Hills in Valleys", "Upper Slopes, Mesas", and "Open Slopes", were excluded from the analysis, since they are almost unaffected by gold mining (Figure 3c). The only exceptions are a few mining areas associated with ore deposits, which are located outside rivers and can be missed if only valleys are considered. To avoid missing them, the data on mining allotments were added to the analysis, regardless of their belonging to landform classes. Thus, we selected all bare areas located in valleys as well as within mining allotments. The polygons consisting of one or two Landsat pixels ($\leq$1800 m^2) were removed from the resulting dataset. The mining sites located along each unique river were dissolved.

The discrimination of natural alluvial deposits from mining sites is challenging since alluvial deposits are widespread in river valleys (including those affected by gold mining) and have the same spectral properties as mining-impacted areas (Figure 2). Therefore, these two classes were distinguished manually, based on textural and contextual features of mining sites. In particular, river valleys impacted by alluvial gold mining, unlike non-transformed ones, are characterized by large areas with removed vegetation, numerous

man-made dams and reservoirs, and heavily transformed channels, which are well-detected on both medium and high-resolution satellite images (Figure 3). The resulting dataset includes only mining areas with completely removed vegetation, while large man-made reservoirs and historical mining areas with recovering vegetation have been excluded.

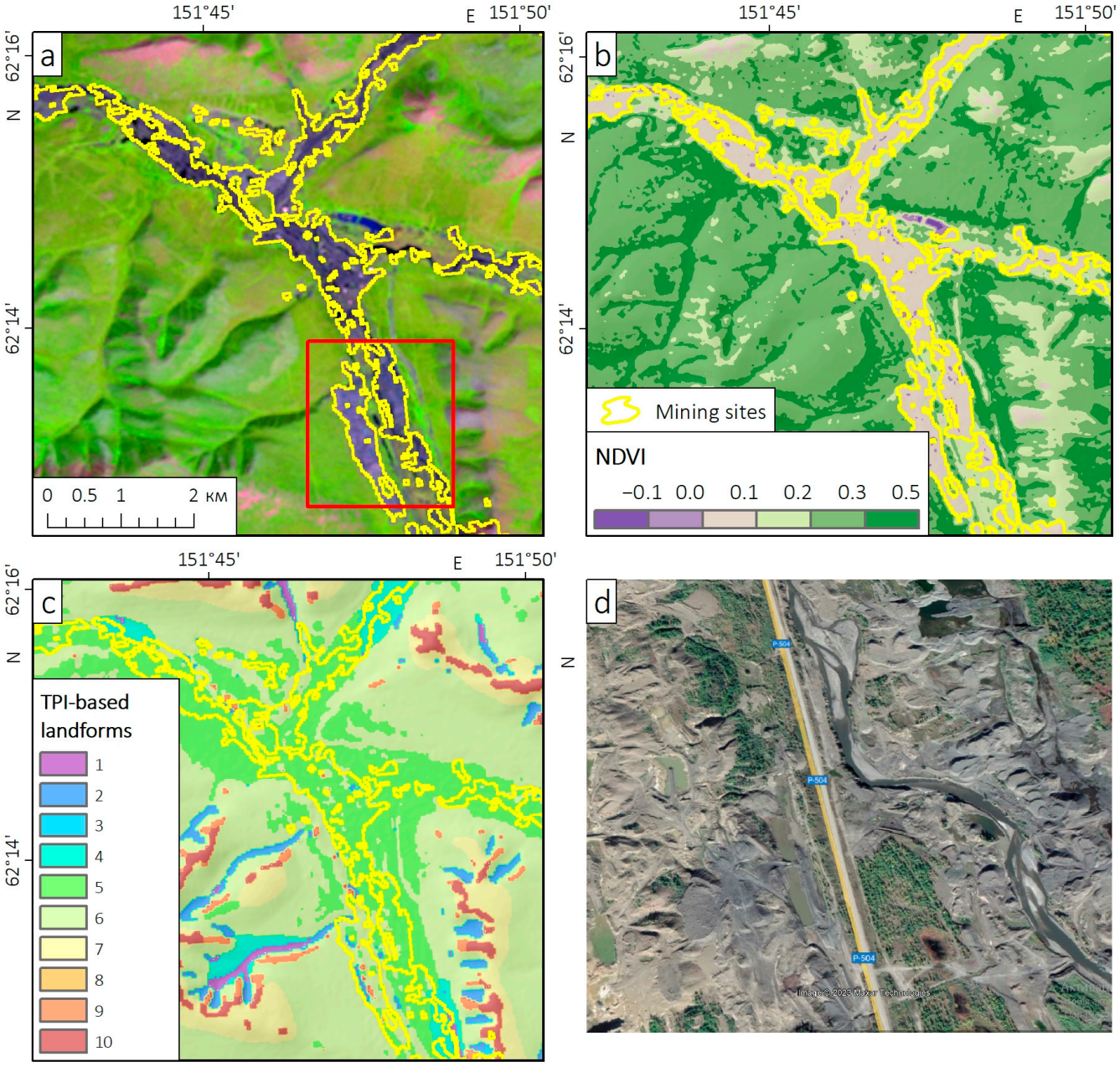

Figure 3. Identification of mining sites near Orotukan settlement, the Magadan region: Landsat-7 ETM+ image obtained on 10 July 2000, band combination 5-4-3 (**a**), Normalized Difference Vegetation Index (**b**), TPI-based landform classification (**c**) and high-resolution image from Google Earth (**d**) (the area is shown with a red rectangle). Landform classes are 1—Canyons, Deeply Incised Streams, 2—Midslope Drainages, Shallow Valleys, 3—Upland Drainages, Headwaters, 4—U-shaped Valleys, 5—Plains, 6—Open Slopes, 7—Upper Slopes, Mesas, 8—Local Ridges, Hills in Local Ridges, Hills in Valleys, 9—Midslope Ridges, Small Hills in Plains, 10—Mountain Tops, High Ridges.

2.2.4. Identification of Mining Sites from Sentinel-2 Images

We used as initial data 26 pairs of Sentinel-2 images with a difference in imagery dates of 4–6 years. The first images in pairs were obtained in 2016 (15 images) or 2017−2018

(11 images), and the second images were obtained in July–August 2022. To detect mining sites using Sentinel-2 images, a geoprocessing model was compiled in ArcGIS ModelBuilder. As with Landsat images, mining areas were detected based on NDVI threshold values, but the difference in NDVI in each pair of images was additionally calculated to detect mining expansion over the past 4–6 years. NDVI was calculated as (B8 − B4)/(B8 + B4), where B8 and B4 are near-infrared and red bands of the Sentinel-2 MSI images, respectively, which have a spatial resolution of 10 m.

Expansion of gold mining leads to the total removal of a canopy and substantially decreases NDVI. We calculated the NDVI difference from each pair of Sentinel-2 images and selected the areas where NDVI substantially decreased (by 0.3 or more) between 2016−2018 and 2022, and NDVI in 2022 was $\leq$0.1. Water bodies were excluded using the threshold value of the Normalized Difference Water Index (NDWI) [59], equal to 0.1. NDWI was calculated as (B3 − B8)/(B3 + B8), where B3 and B8 are green and shortwave infrared bands of Sentinel-2 MSI images, respectively, with 10 m spatial resolution.

Thus, we detected the areas where vegetation canopy was removed between 2016–2018 and 2022 by mining or other agents. Threshold values of indices are set as model parameters and may be corrected if the area of mining sites is overestimated or underestimated. Primary visual inspection of mining area identification results was performed using Sentinel-2 images.

A strong decrease in NDVI may be associated with both gold mining and other agents like wildfires, the formation of islands and shoals on rivers, and even mudflow or debris flow plumes. We used additional data, namely TPI-based landform classification and mining allotments to discriminate mining sites from other classes (see Section 2.2.3 for details). In particular, bare areas located both outside the mountain allotments and river valleys were excluded. Finally, alluvial deposits were discriminated from mining sites manually. Thus, we detected all land-cover changes, presumably associated with gold mining.

In addition, all barren lands (with NDVI $\leq$ 0.1) were detected on the images obtained in 2022. Among them, we selected the areas that intersected or had a common border with previously identified mining-related land-cover changes, and located within river valleys or mining allotments (Figure 4). Other areas were excluded from the analysis. The obtained dataset, after excluding the areas not related to gold mining (in particular, alluvial deposits), contains all gold-mining sites with totally removed vegetation for 2022.

2.2.5. Validation of Identified Mining Sites Using High-Resolution Image

The used method of mining site identification from both Landsat and Sentinel-2 images has several obvious limitations. First, only the areas with totally removed vegetation are taken into account. Second, several impacted areas may be missed if there has been no mining activity in the last 4–6 years. Third, a substantial part of mining sites is covered by man-made water bodies, and they are also excluded from analysis since there are no obvious ways to distinguish them from natural ones. In addition, finally, manual discrimination of natural alluvial deposits and mining sites is time-consuming since both these land-cover types are widespread along the same rivers. To evaluate the method's limitations in more detail, we validated the detected mining areas using high-resolution imagery from Google Earth, obtained on 21 June 2020.

We selected a validation plot with a total area of 6320 ha^2, located along the Berelekh River near the town of Susuman, where gold mining has been developing for a long time. We delineated manually from high-resolution images the mining-impacted areas and separated them into two classes, namely bare areas and man-made water bodies. Their area reaches 738 ha and 382 ha, respectively (1120 ha in total) according to high-resolution images. The area of mining sites located within the validation plot, according to the Sentinel-2 image, is 887 ha (except for the areas where mining began after 2020). Thus, the mining area according to the Sentinel-2 image is underestimated by 21% in comparison with the validation dataset.

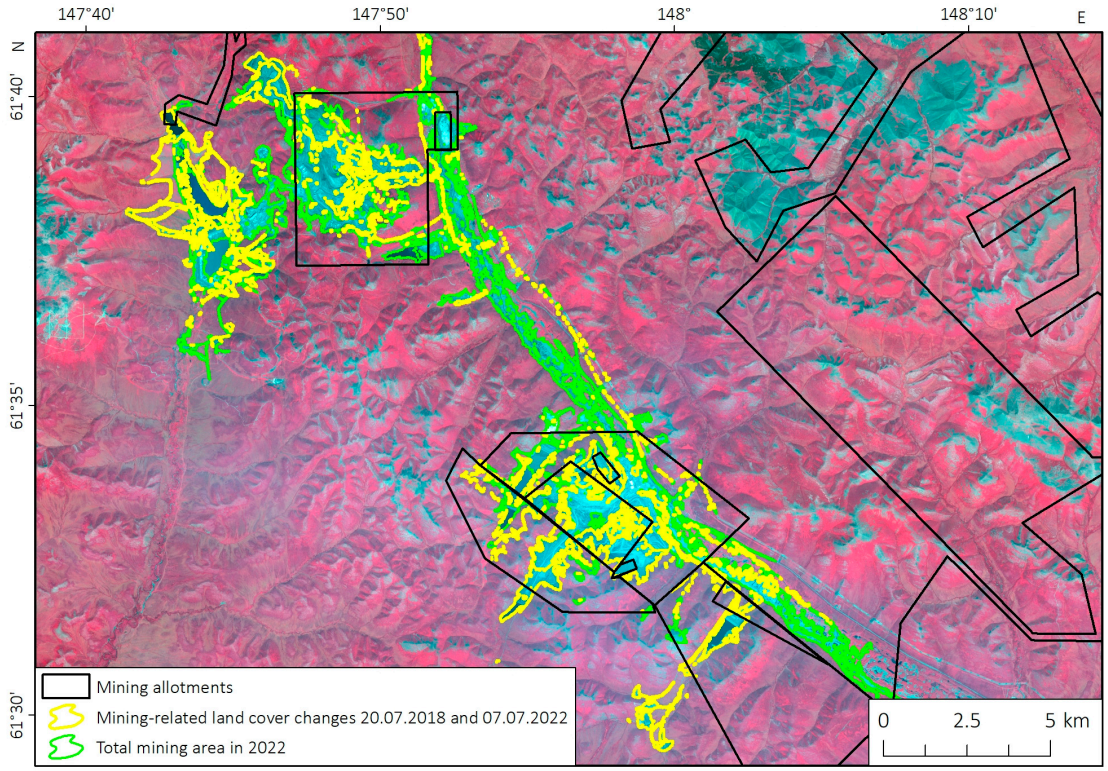

Figure 4. Expansion of alluvial and ore gold-mining areas at Natalkinskoe gold deposit (the Magadan region). The total area of degraded lands and land-cover changes over 2018–2022 are shown.

We overlapped mining areas delineated from the high-resolution image (validation data) with the same obtained according to the Sentinel-2 image (examined data). The matched area (true positive, TP) is 653.5 ha, while precision and recall are 0.736 and 0.583, respectively. Please note that 476 ha of TP area falls to bare lands, and the other 177 ha are man-made water bodies according to high-resolution imaging. Therefore, these water bodies are too small and complex in shape to be identified from Sentinel-2 images. Thus, 262 ha of bare areas are missed, and 233 ha of them are falsely detected from the Sentinel-2 images. These differences can be explained mainly by the different spatial resolutions of the Sentinel-2 image and the image from Google Earth (10 m and 0.5 m, respectively), and by the above-mentioned limitations of the NDVI-based method.

2.3. Identification of Vegetation Recovery on Mining-Impacted Lands

Vegetation recovery in gold-mining areas is strongly determined by the type of deposit. In ore deposits, where gold ores are mined in quarries, the waste rock dumps usually contain plant seeds, which contribute to the beginning of vegetation regeneration in a short time after the end of mining. On the contrary, in alluvial deposits, they consist of well-washed gravel, in which plant seeds are absent. Revegetation in such mining areas takes several decades [60].

The identification of revegetation processes in mining areas was performed in two stages: detection of the areas recovered by vegetation, and analysis of NDVI trends for the detected areas over the past 20 years. We considered vegetation recovery for the most impacted basin of the Berelekh River (see Section 3 for details).

Data processing was performed using the Google Earth Engine [61] and included such steps as the compilation of the initial dataset consisting of Landsat-5,7,8 collections, cloud masking, and the calculation of NDVI values. In total, we used 10 images from Landsat-7 (for 2000), 27 images from Landsat-5 (for 2009), and 31 images from Landsat-8 (for 2021). All images were obtained for the period from 15 July to 10 September, which approximately corresponds to the vegetation period in the studied basin of the Berelekh River. Annual

NDVI maximums were calculated for each pixel. Next, a multi-temporal image of three NDVI maximum bands calculated for 2000 (according to Landsat-7 data), 2009 (according to Landsat-5 data), and 2021 (according to Landsat-8 data) was created (Figure 5d). A 10-year time step was chosen since the revegetation process in the dumps takes a long time [60].

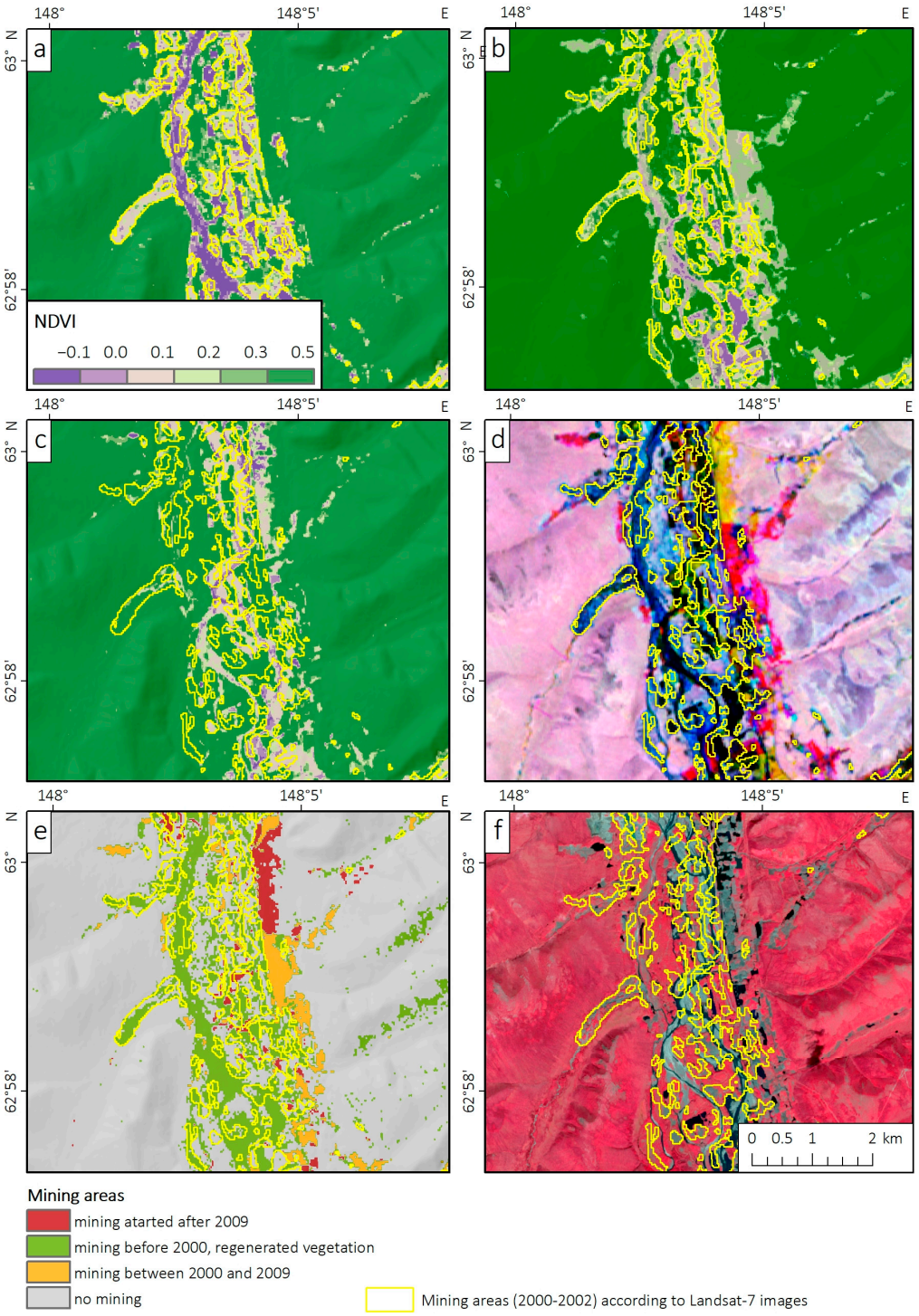

Figure 5. Identification of vegetation recovery on mining sites: NDVI values calculated for the summer of 2000 (**a**), 2009 (**b**), and 2021 (**c**), RGB composite of NDVI for 2000, 2009, and 2021, regenerated vegetation is shown in blue colors (**d**), CART classification outputs (**e**) and Sentinel-2 images obtained in July 2022 (**f**).

The red, green, and blue bands of the resulting image are the maximum NDVI values for 2000, 2009, and 2021, respectively. The areas where NDVI in 2009 and 2021 was substantially lower than in 2000 are shown in red colors and indicate the gold mines where mining started between 2000 and 2009. Yellow colors showed the areas where NDVI decreased between 2009 and 2021, and, therefore, gold mining started in this period. Blue colors correspond to the areas where NDVI in 2021 was substantially higher than in 2000 and 2009, which indicates vegetation recovery in historical mining areas.

Then, we used the binary decision-tree algorithm Classification and Regression Tree (CART) [62] with training in the Google Earth Engine to identify the areas where the revegetation process has been observed over the past 20 years. The input NDVI composite was classified into four classes, namely the areas where vegetation has been removed due to gold mining in 2000−2009 (1), the same for 2009–2021 (2), the areas where revegetation has been observed between 2000 and 2021 (3), and the areas without substantial NDVI changes (4). For each class, we compiled a training sample consisting of 120 pixels. A fragment of the classification result is shown in Figure 4e. Class #3 (areas with recovering vegetation) was extracted for further analysis.

3. Results

3.1. Overview of Mining-Related Land-Cover Changes in the Magadan Region

Overall, for the Magadan region, the area of gold-mining sites according to the Landsat-7 ETM+ images obtained in 2000–2002 was estimated as 41,206 ha. According to the Sentinel-2 images obtained in 2022, it had increased to 72,602 ha. Comparing the Sentinel-2 images obtained in 2016–2018 and 2022, we found 720 areas of mining-related vegetation loss associated with both new mines and expanded mine workings, where mining started in previous years. Their total area is 26,031 ha (35.8% of the total impacted area in 2022).

About 82.5% of the total mining areas identified from Sentinel-2 images of 2022, and 80.5% of new ones (when mining started between 2016–2018 and 2022) are located within mining allotments. The remaining 19.5% of mining areas, located outside of them, can be partially associated with the newest mine workings (where mining started in 2022) since the dataset of mining allotments is valid for 2021. Several gold mines located outside of the allotments may be illegal, but the available data do not allow us to assess the significance of illegal mining in the Magadan region.

About 15,610 ha of mining areas have been identified both from Landsat and Sentinel-2 images. Thus, these areas have low NDVI ($\leq$0.1) both in 2000–2002 and in 2022, which indicates the lack of revegetation after mining for at least 20 years. However, the results of the overlay of mining areas detected in 2000–2002 and 2022 should be considered with caution, since input datasets are based on satellite images of different spatial resolutions (30 m and 10 m, respectively).

River systems are mostly impacted by gold mining, in comparison with other components of the natural environment [12,36]. Therefore, we mapped mining areas in the context of river basins. In particular, the proportion of mining areas in relation to the total basin area was calculated for both 2000–2002 (Landsat-based dataset), for 2022 (Sentinel-2-based dataset), and for mining sites delineated from Sentinel-2 images between 2016–2018 and 2022. The calculation was performed for 319 basins in the Magadan region with an area of 200 km^2 or more, which were delineated automatically from the ALOS WTD digital surface model, with the use of ArcGIS Spatial Analyst (Hydrology tools). The results are shown in Figures 6–8.

Mining-impacted areas are concentrated in the western part of the Magadan region, namely in the Susuman, Ten'kinsky, and Yagodninsky municipal districts, which are related to the Kolyma gold belt [63]. Thus, gold mining along the Berelekh River and its tributaries began over 80 years ago and continues at the present [37], which determines the most severe impact on the natural environment. According to the Sentinel-2 images of 2022, mining sites with totally removed vegetation canopy occupy 1.69% of the total area of the Berelekh River basin (~16,500 ha) and 1.47% of the adjacent Debin River basin (~8000 ha),

which makes up one third of the total mining area in the Magadan region. In several sub-basins, the contribution of severely impacted mining areas reaches 5% (Figure 7). On the contrary, in other parts of the region, gold production is carried out in isolated deposits, and the proportion of the impacted area is less than 1%, except for one basin near the town of Omsukchan.

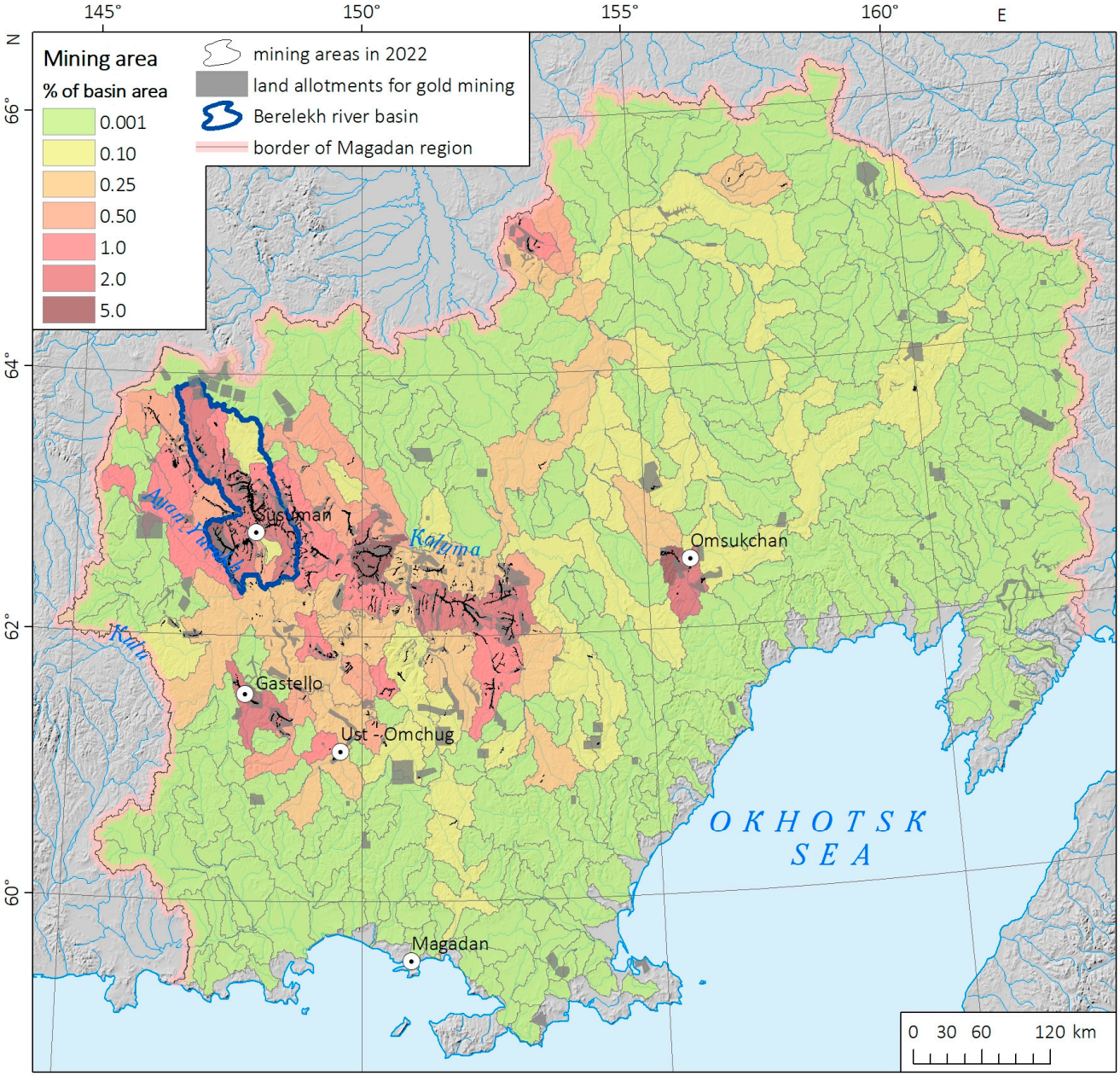

Figure 6. The total area of mining sites according to the Landsat images obtained in 2000–2002, calculated for large river basins (S > 200 km^2) in the Magadan region. The most impacted basin of the Berelekh River is shown.

The spatial distribution of mining-impacted areas has had no significant changes over the past 20 years (Figure 8). Mining area substantially increased in the basins of the Berelekh, Debin, and Ten'ka Rivers, where numerous placer and ore gold deposits have been developed for a long time. The observed increase in mining areas is in line with substantially increased gold production in the Magadan region over the past 10 years, especially for ore gold deposits. Thus, ore gold production increased from 6.9 tons to 31.78 tons, and placer one—from 14.5 tons to 19.65 tons in 2013 and 2022, respectively [38], resulting

in a substantial increase in impacted areas. Thus, the mining area in the basin of Ten'ka River (S = 1834 km^2) almost tripled (1843 ha in 2000–2002 and 5116 ha in 2022) due to active mining in the largest ore gold deposits "Natalka" and "Pavlik", and associated placers.

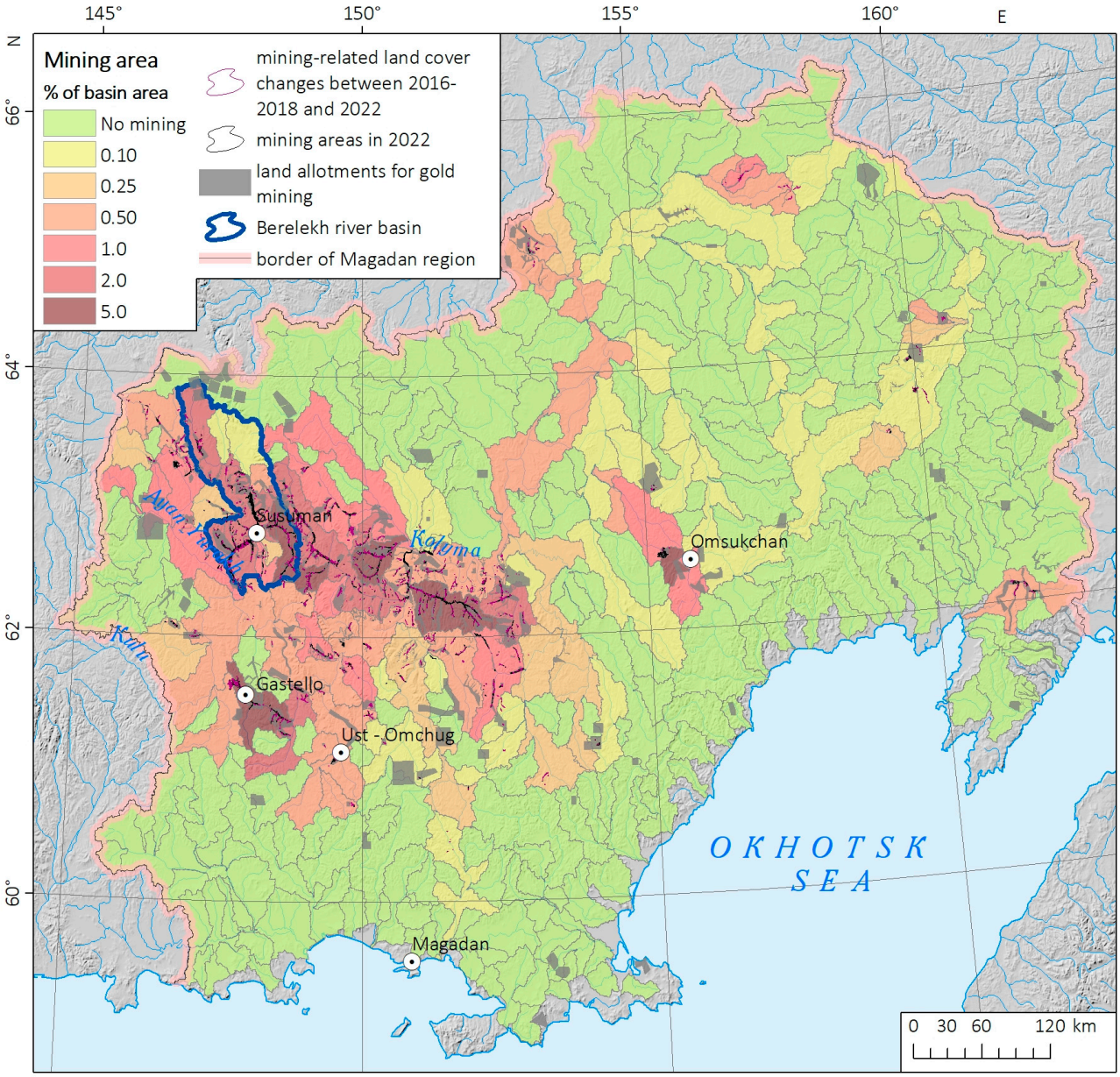

Figure 7. The total area of mining sites according to Sentinel-2 images obtained in 2022, calculated for large river basins (S > 200 km^2) in the Magadan region. The most impacted basin of the Berelekh River is shown.

The most substantial impact of gold mining on terrestrial ecosystems is associated with alluvial mining in river valleys. We estimated the degree of transformation of river valleys in the Berelekh and Debin River basins, mostly impacted by gold mining compared with other river basins of the region. Using the ALOS WTD digital surface model and Hydrology tools in the ArcGIS Spatial Analyst, we identified the thalwegs with a catchment area of more than 100 km^2 and a length of more than 10 km (the StreamLink tool was used). Then, 500 m buffers were built around each thalweg, and the contribution of mining areas with removed vegetation canopy was calculated for each buffer (Figure 9). We found that mining areas within 500-m buffers along rivers (with totally removed vegetation) cover 4.55% and 6.15% in the Berelekh and Debin basins, respectively. The upper part of the

Berelekh River basin is still low impacted by gold mining, while in the Debin River basin, mining areas are distributed more evenly. Floodplains of the Berelekh and Debin Rivers themselves are impacted much more strongly (mining areas with removed vegetation occupy 16.0% and 11.2% of them, respectively). Along with impacted land, a substantial area is occupied by man-made reservoirs, which is not taken into account as mining areas. Considering both present and historical mine workings (where the vegetation is already recovered), as well as man-made reservoirs, the floodplains of both Berelekh and Debin Rivers are transformed by more than 50%, and up to 90% in several of their tributaries (with the proportion of bare areas reaching 25–27%). Such severe impact on floodplains leads to a substantial increase in water turbidity, which is especially typical for the Berelekh River [39].

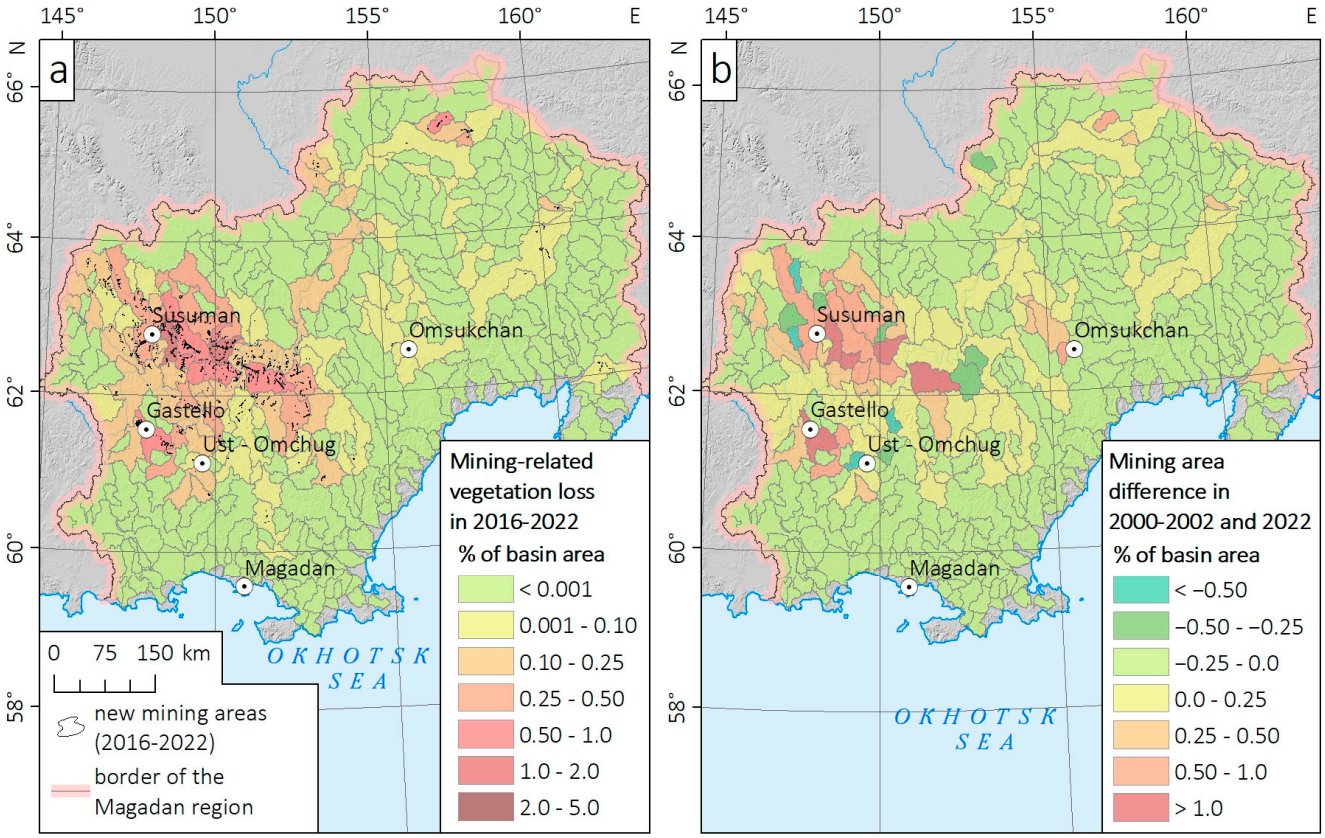

Figure 8. Mining-related vegetation loss according to Sentinel-2 images (**a**) and changes in mining areas between 2000–2002 and 2022 (**b**).

We also used two land-cover/land-use (LCLU) maps namely GlobCover-2009 [54] and a satellite-based map of the vegetation cover of Russia [55] to determine LCLU types mostly impacted by gold mining. Both maps have moderate spatial resolution (230 and 350 m, respectively), but are characterized by enough detailed classification of the LCLU types. In addition, these maps have been developed in 2008 and 2016, respectively, which makes it possible to determine LCLU types impacted by gold mining in 2016–2022 (Tables 2 and 3).

Table 2. LCLU classes impacted by gold mining in the Magadan region in 2016–2022, according to the GlobCover-2009 map [54]. Classes with a total area of <10 km^2 are not shown.

Land-Cover Class	Total Area, km^2	Impacted Area, km^2
Bare areas	38,091.1	14.52
Closed (>40%) broad-leaved deciduous forest (>5m)	678.8	–
Closed to open (>15%) mixed broad-leaved and needle-leaved forest (>5m)	2639.7	–

Table 2. *Cont.*

Land-Cover Class	Total Area, km^2	Impacted Area, km^2
Mosaic forest or shrubland (50–70%)/grassland (20–50%)	44,409.4	12.04
Mosaic grassland (50–70%)/forest or shrubland (20–50%)	59,217.1	31.15
Open (15–40%) needle-leaved deciduous or evergreen forest (>5m)	234,777.0	182.22
Permanent snow and ice	348.5	–
Sparse (<15%) vegetation	78,127.4	19.94
Water bodies	3112.3	–

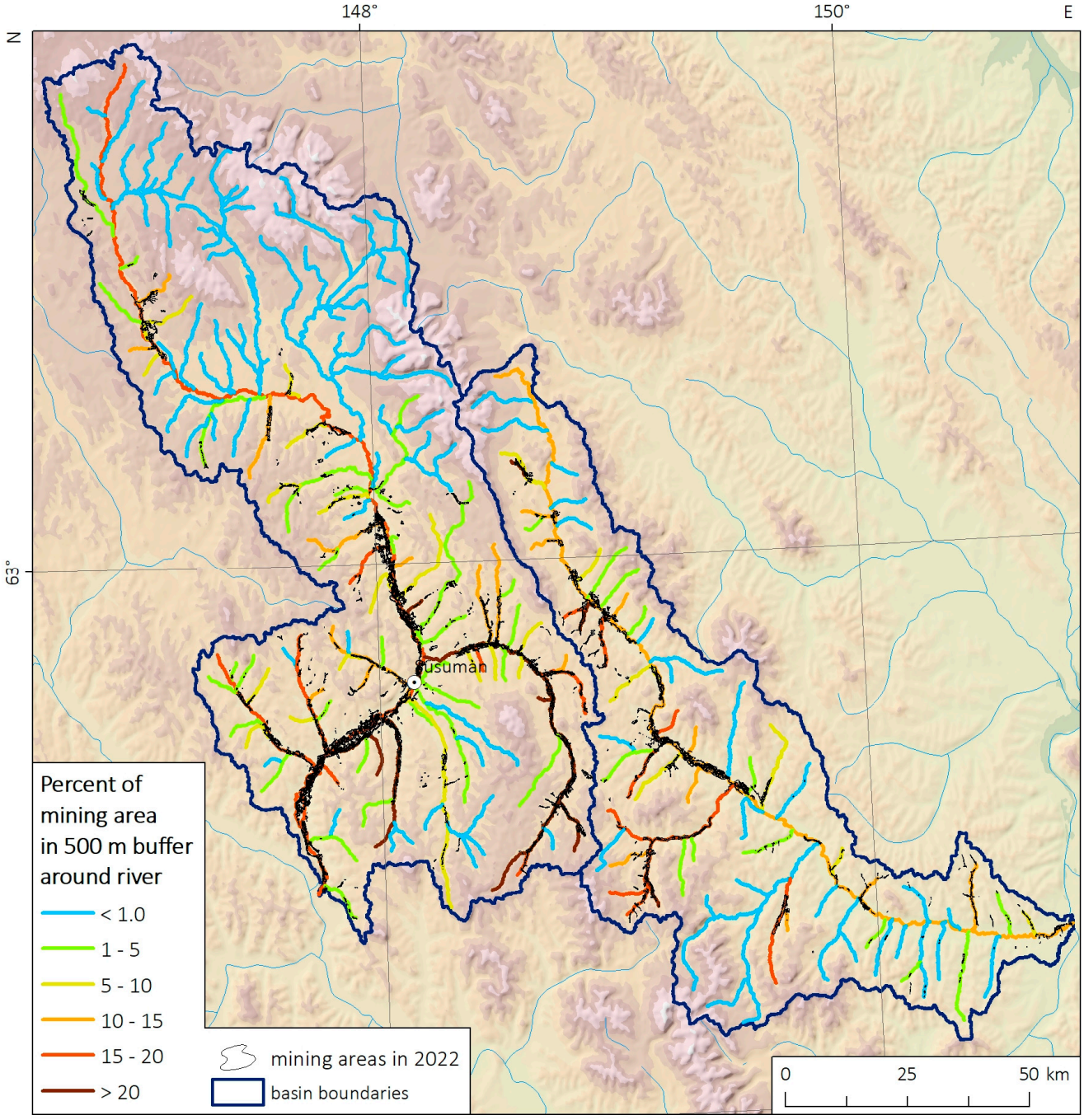

Figure 9. Percentage of mining areas in 500 m buffer around rivers, calculated according to Sentinel-2 images of 2022 for the most impacted basins of Berelekh and Debin Rivers.

Table 3. LCLU classes impacted by gold mining in the Magadan region in 2016–2022, according to the map of the vegetation cover of Russia [55]. Classes with a total area of <10 km^2 are not shown.

Land-Cover Class	Total Area, km^2	Impacted Area, km^2
Burned areas	2364.7	1.1
Coniferous evergreen shrubs	104,776.0	71.9
Coniferous Larch forests	54,080.1	27.3
Deciduous forests	1114.9	–
Grasslands	208.9	–
Mixed forests	12.2	–
Mixed forests with coniferous dominating	161.8	–
Mixed forests with deciduous dominating	54.4	–
Open ground and rocks	43,549.6	16.4
Sparse larch forests	65,948.9	41.5
Shrublands	17,984.3	8.2
Swamps	33,368.9	41.7
Tundra	137,571.0	49.1
Urban areas	14.0	–
Water bodies	1535.4	–

According to both LCLU maps, most of the area impacted by gold mining after 2016 falls on larch forests (northern taiga) and coniferous evergreen shrubs (cedar elfin), widespread in the subarctic climate of the Magadan region in river valleys and the lower parts of mountain slopes. Thus, according to the GlobCover-2009 data, about 51% of the study area and over 70% of mining-impacted areas (after 2016) are covered by sparse coniferous forests. According to the vegetation map of Russia [55], which provides a more detailed LCLU classification, the main part of the impacted area falls on evergreen coniferous shrubs, larch forests, and swamps (note that floodplain ecosystems can also be classified as swamps). In relative terms, swamps and floodplain ecosystems are most impacted (0.13% of their total area), while for other LCLU types, the impacted areas do not exceed 0.07%. It should be noted that only a mining area with removed vegetation canopy after 2016 was estimated here, while the total area is substantially larger.

3.2. Assessment of Vegetation Recovery at Historical Gold-Mining Sites in the Berelekh River Basin

We estimated the total area of the vegetation recovery at gold-mining sites in the Berelekh River basin as 19,900 ha, while the new area impacted by gold mining between 2000 and 2021 is 29,600 ha (Figure 10). This is substantially higher than the Sentinel-2-based estimate (16,500 ha) since we did not exclude from this assessment man-made reservoirs, which are widespread in gold-mining sites (see Section 2.2.5 for details).

To confirm the vegetation recovery process, we selected three test sites classified as recovered vegetation (shown in Figure 10). For each of them, the average NDVI was calculated for July and August for the periods 1999–2022 (based on Landsat-7 images) and 2014–2022 (based on the Landsat-8 images). In total, 188 NDVI values were extracted from the Landsat-7 data, and 135 from the Landsat-8 data. Figure 11 shows NDVI calculated from the Landsat-7 images. We calculated trends for both annual average and maximum NDVI values using the Theil–Sen estimator, and significance was obtained with the nonparametric Mann–Kendall test. Both trends are statistically significant at a significance level of 0.05, and Sen's slope coefficients are 0.018 and 0.020, respectively, for annual average and maximum NDVI values. Therefore, we found that vegetation recovery is observed according to satellite images in a substantial area affected by gold mining before 2000, and the area recovered by vegetation is comparable to the area impacted by mining over the past 20 years. It is of note that most of the areas recovered by vegetation are located near the town of Susuman, while new mining areas are more distant from it (located in harder-to-reach places).

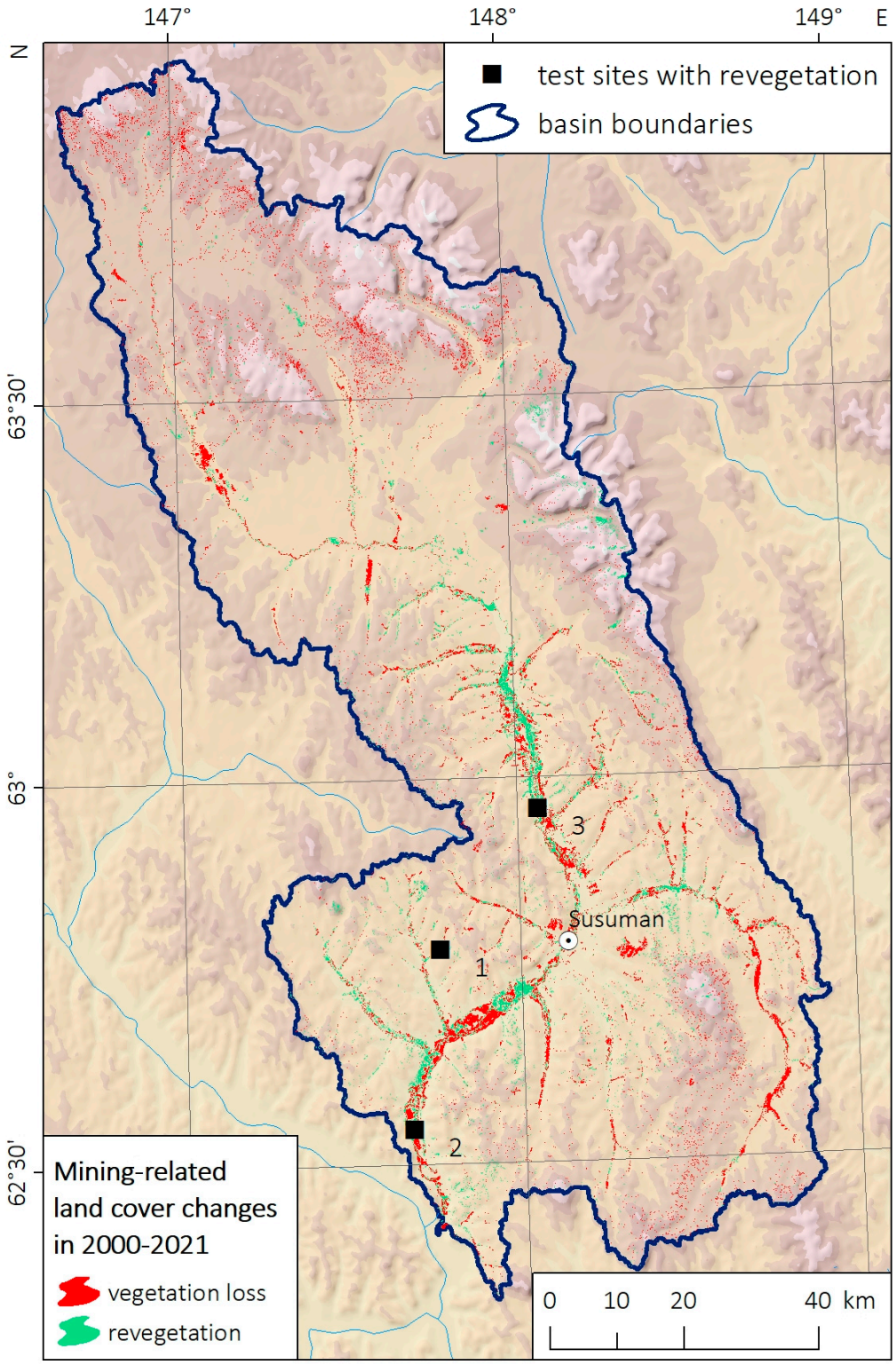

Figure 10. Areas of mining-related vegetation loss and recovery in the Berelekh River basin in 2000–2021.

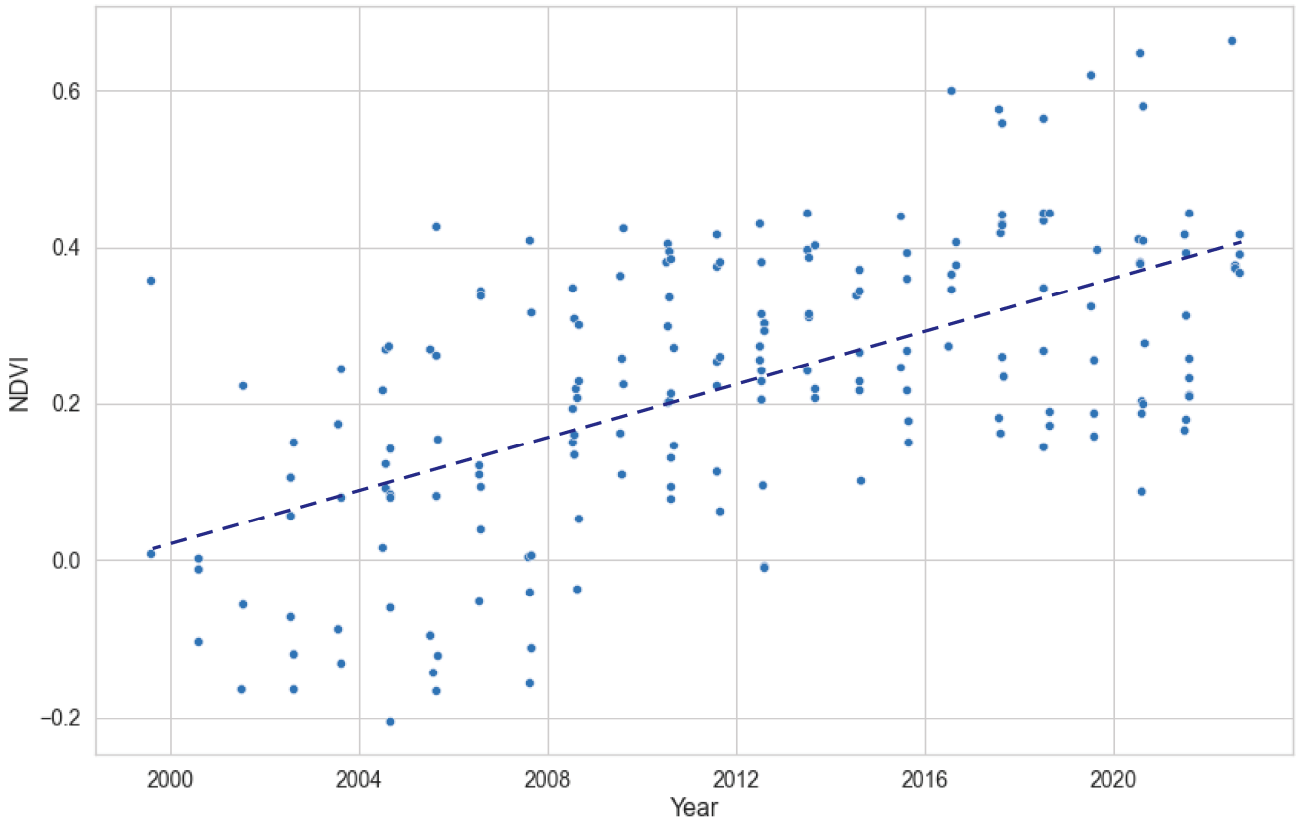

Figure 11. Summertime NDVI obtained from Landsat-7 images in July–August 2000–2022 on three sites with recovered vegetation.

4. Discussion and Conclusions

Gold mining at ore and alluvial deposits is a key sector of the industry both in the Magadan region and in other parts of Eastern Siberia and the Russian Far East. Total gold production in Russia increased by 1.6 times from 2011 to 2020 and exceeded 300 tons per year, while gold production from alluvial placers increased from 60.5 tons in 2011 to 82.4 tons in 2020 [64]. Thus, gold mining's impact on the ecosystems of rivers and floodplains also substantially increased. At present, Russia does not have a state system for monitoring the impact of gold mining on the environment. In Eastern Siberia and the south of the Far East, satellite-based monitoring was performed by volunteers with the support of the World Wildlife Fund [59], and an inventory of impacted lands has been completed only for the Amur River basin [36]. The Magadan region, like other parts of northeastern Russia, remained out of the focus of both scientific and volunteer projects in the field of assessment of gold-mining impacts, although the placer gold production here is greater than the same in the southern part of the Russian Far East. In addition, the Magadan region is characterized by a subarctic climate and continuous permafrost, which prevents vegetation recovery on mining sites [43].

This study provides a detailed overview of land-cover changes associated with gold mining in the Magadan region in the 21st century. We focused only on land degradation and vegetation recovery on mining sites and did not consider other effects of gold mining, which can be also observed from satellite images, like water contamination with suspended solids [18,19]. In our previous study [39], we showed that the lack of gauging stations measuring the total suspended solid (TSM) downstream of gold-mining sites, along with the changes in water turbidity associated with summer rain floods substantially complicates the validation of satellite-based estimates of river's contamination. However, mining-impacted areas calculated in the context of river basins (Figures 6–8) can be used as a proxy indicator to assess the impact of gold mining on stream systems and water quality.

In line with the above-mentioned increase in placer gold production, our results indicate a substantial increase in mining-impacted areas in the Magadan region between 2000–2002 and 2022. The estimated area of gold-mining sites in 2000–2002 was 41,206 hectares, and it increased to 72,602 hectares according to Sentinel-2 images obtained in 2022. The study also identified 720 areas of mining-related vegetation loss between 2016–2018 and 2022, accounting for 35.8% of the total impacted area in 2022. The spatial distribution of mining-impacted areas has not changed significantly over the past two decades, with the most substantial impact observed in the basins of the Berelekh, Debin, and Ten'ka Rivers.

Most of the mining areas identified in 2022, as well as the new ones (where mining began after 2016–2018), were located within mining allotments, accounting for approximately 82.5% and 80.5%, respectively. However, about 19.5% of mining areas were located outside of the allotments, which could be associated with the newest mine works that started in 2022, and (to a lesser degree) illegal mining.

The study also assessed the degree of transformation of river valleys in the Berelekh and Debin River basins, and the large tributaries of the Kolyma River, which were heavily impacted by gold mining. The floodplains of these rivers showed substantial mining-related changes, with mining areas with totally removed vegetation canopy occupying 16.0% and 11.2% of the floodplains of the Berelekh and Debin Rivers, respectively. The transformation of these floodplains resulted in increased water turbidity, particularly noticeable in the Berelekh River [39].

The analysis of land-cover types impacted by gold mining revealed that most mining-impacted areas after 2016 were covered by larch forests and coniferous evergreen shrubs, prevalent in the subarctic climate of the Magadan region, particularly in river valleys and lower mountain slopes.

It is of note that the used method of mining site identification from both Landsat and Sentinel-2 images has several limitations, which lead to the underestimation of impacted areas. Thus, we present the lower-boundary estimate of the area impacted by gold mining, which, however, reflects the main patterns in the spatial distribution of the impact of gold mining and its change over the past 20 years.

Along with land degradation, the study assessed vegetation recovery at historical gold-mining sites in the Berelekh River basin. The total area of vegetation recovery was estimated at 19,900 hectares, while the area impacted by gold mining between 2000 and 2021 was 29,600 hectares. The analysis of NDVI values indicated substantial vegetation recovery in areas affected by gold mining before 2000, which is comparable in size to the areas impacted by mining over the past 20 years.

Overall, these findings highlight the extent of land-cover changes related to gold-mining activities in the Magadan region, emphasizing the concentration of mining sites in specific areas and the importance of ongoing monitoring and environmental management practices in mitigating these impacts. The assessment of the degree of land degradation in the Magadan region cannot be compared to other similar regions in Russia as much in detail, as such assessments were conducted only for the southern part of the Russian Far East [65–67]. Thus, in the Amur River basin, 1123 mining sites in river floodplains covering an area of 2111 km^2 were found based on Landsat-5 TM images. The total length of impacted river valleys was estimated as 6537 km (1.6% of the total length of the rivers in the Amur basin) [36,67]. An annual increase in the area impacted by gold mining in alluvial placers was estimated at 15 km^2 only in the Amur region [68]. The degree of land degradation was also analyzed in other regions like middle Yenisey [6] and Buryatia [69], but only at individual gold-mining sites.

Yu et al. [70], showing the promising capabilities of remotely sensed data in understanding the dynamics of mining activities on a global scale, unveiled the trends regarding surface mines in North America, South America, and Asia. It was observed that between 1980 and 2013, a substantial proportion of surface mines in North America underwent size reduction, indicating successful rehabilitation efforts. In contrast, Asia and South America saw notable expansions in mining areas, signifying increased mining activities in those

regions. The consideration of the region's harsh climatic conditions and permafrost and their influence on vegetation restoration, as well as the impact on stream systems, including pollution with suspended solids, is crucial to obtaining an understanding of the unique challenges and potential environmental consequences not only on a regional scale but also a global one.

Author Contributions: Conceptualization, O.M.; methodology, A.S. and P.I.; software, P.I.; investigation, A.S., P.I. and M.M.; data curation, A.S., P.I. and A.Z.; writing—original draft preparation, A.S. and P.I.; writing—review and editing, O.M. and A.Z.; visualization, A.S. and P.I.; supervision, O.M.; project administration, O.M.; funding acquisition, O.M. All authors have read and agreed to the published version of the manuscript.

Funding: The study was carried out with the support of St. Petersburg State University Project ID 95413735.

Data Availability Statement: All data are available upon request to the corresponding author.

Conflicts of Interest: The authors declare no conflict of interest. The funders had no role in the design of the study; in the collection, analyses, or interpretation of data; in the writing of the manuscript, or in the decision to publish the results.

References

1. Hooke, R.L.; Martín-Duque, J.F.; Pedraza, J. Land transformation by humans: A review. *Geol. Soc. Am. Today* **2012**, *22*, 4–10. [CrossRef]
2. Chetty, S.; Pillay, L.; Humphries, M.S. Gold mining's toxic legacy: Pollutant transport and accumulation in the Klip River catchment, Johannesburg. *S. Afr. J. Sci.* **2021**, *117*, 8668. [CrossRef] [PubMed]
3. Bridge, G. Contested Terrain: Mining and the environment. *Annu. Rev. Environ. Resour.* **2004**, *29*, 205–259. [CrossRef]
4. Laker, M.C. Environmental Impacts of Gold Mining—With Special Reference to South Africa. *Mining* **2023**, *3*, 205–220. [CrossRef]
5. Guidebook for Evaluating Mining Project EIAs. Environmental Law Alliance Worldwide (ELAW). 2010. Available online: https://www.elaw.org/mining-eia-guidebook (accessed on 30 June 2023).
6. Schueler, V.; Kuemmerle, T.; Schröder, H. Impacts of surface gold mining on land use systems in Western Ghana. *Ambio* **2011**, *40*, 528–539. [CrossRef]
7. Kharuk, V.L.; Ranson, K.J.; Im, S.T.; Fedotova, E.V. Impact of Gold Mining on Middle Siberian Taiga Landscapes from Landsat-7 Data. *Mapp. Sci. Remote Sens.* **2002**, *39*, 139–156. [CrossRef]
8. Obodai, J.; Adjei, K.A.; Odai, S.N.; Lumor, M. Land use/land cover dynamics using Landsat data in a gold mining basin-the Ankobra, Ghana. *Remote Sens. Appl. Soc. Environ.* **2013**, *13*, 247–256. [CrossRef]
9. Finer, M.; Novoa, S. *MAAP Synthesis # 1: Patterns and Drivers of Deforestation in the Peruvian Amazon*; ACCA: Lima, Peru, 2015.
10. Caballero Espejo, J.; Messinger, M.; Román-Dañobeytia, F.; Ascorra, C.; Fernandez, L.E.; Silman, M. Deforestation and Forest Degradation Due to Gold Mining in the Peruvian Amazon: A 34-Year Perspective. *Remote Sens.* **2018**, *10*, 1903. [CrossRef]
11. Jarsjö, J.; Chalov, S.R.; Pietroń, J.; Alekseenko, A.V.; Thorslund, J. Patterns of soil contamination, erosion and river loading of metals in a gold mining region of northern Mongolia. *Reg. Environ. Chang.* **2017**, *17*, 1991–2005. [CrossRef]
12. Glotov, V.E.; Chlachula, J.; Glotova, L.P.; Little, E. Causes and environmental impact of the gold-tailings dam failure at Karamken, the Russian Far East. *Eng. Geol.* **2018**, *245*, 236–247. [CrossRef]
13. Gallo Corredor, J.A.; Lizeth Vargas González, G.; Velasco Granados, M.; Gutiérrez, L.; Pérez, E.H. Use of the gray water footprint as an indicator of contamination caused by artisanal mining in Colombia. *Res. Policy* **2021**, *73*, 102197. [CrossRef]
14. Maus, V.; Giljum, S.; da Silva, D.M.; Gutschlhofer, J.; da Rosa, R.P.; Luckeneder, S.; Gass, S.L.B.; Lieber, M.; McCallum, I. An update on global mining land use. *Sci. Data* **2022**, *9*, 433. [CrossRef] [PubMed]
15. S&P Global Market Intelligence. SNL Metals and Mining Database. 2023. Available online: https://www.spglobal.com/marketintelligence/en/campaigns/metals-mining (accessed on 30 June 2023).
16. Li, Y.; Zhao, H.; Fan, J. Application of Remote Sensing Technology in Mine Environment Monitoring. *MATEC Web Conf.* **2015**, *22*, 4008. [CrossRef]
17. Moomen, A.-W.; Lacroix, P.; Benvenuti, A.; Planque, M.; Piller, T.; Davis, K.; Miranda, M.; Ibrahim, E.; Giuliani, G. Assessing the Applications of Earth Observation Data for Monitoring Artisanal and Small-Scale Gold Mining (ASGM) in Developing Countries. *Remote Sens.* **2022**, *14*, 2971. [CrossRef]
18. Lobo, F.D.L.; Costa, M.; Novo, E.M.L.M.; Telmer, K. Distribution of Artisanal and Small-Scale Gold Mining in the Tapajós River Basin (Brazilian Amazon) over the Past 40 Years and Relationship with Water Siltation. *Remote Sens.* **2016**, *8*, 579. [CrossRef]
19. Dethier, E.N.; Sartain, S.L.; Lutz, D.A. Heightened Levels and Seasonal Inversion of Riverine Suspended Sediment in a Tropical Biodiversity Hot Spot Due to Artisanal Gold Mining. *Proc. Natl. Acad. Sci. USA* **2019**, *116*, 23936–23941. [CrossRef] [PubMed]
20. Telmer, K.; Stapper, D. *Evaluating and Monitoring Small Scale Gold Mining and Mercury Use: Building a Knowledge-Base with Satellite Imagery and Field Work*; United Nations Industrial Development Organization: Victoria, BC, Canada, 2007.

21. Malik, K.; Robertson, C.; Braun, D.; Greig, C. U-Net convolutional neural network models for detecting and quantifying placer mining disturbances at watershed scales. *Int. J. Appl. Earth Obs. Geoinf* **2021**, *104*, 102510. [CrossRef]
22. Mhangara, P.; Tsoeleng, L.T.; Mapurisa, W. Monitoring the Development of Artisanal Mines in South Africa. *J. S. Afr. Inst. Min. Metall.* **2020**, *120*, 299–306. [CrossRef]
23. Barenblitt, A.; Payton, A.; Lagomasino, D.; Fatoyinbo, L.; Asare, K.; Aidoo, K.; Pigott, H.; Som, C.K.; Smeets, L.; Seidu, O.; et al. The Large Footprint of Small-Scale Artisanal Gold Mining in Ghana. *Sci. Total Environ.* **2021**, *781*, 146644. [CrossRef]
24. Ibrahim, E.; Lema, L.; Barnabé, P.; Lacroix, P.; Pirard, E. Small-Scale Surface Mining of Gold Placers: Detection, Mapping, and Temporal Analysis through the Use of Free Satellite Imagery. *Int. J. Appl. Earth Obs. Geoinf.* **2020**, *93*, 102194. [CrossRef]
25. Nyamekye, C.; Ghansah, B.; Agyapong, E.; Kwofie, S. Mapping Changes in Artisanal and Small-Scale Mining (ASM) Landscape Using Machine and Deep Learning Algorithms—A Proxy Evaluation of the 2017 Ban on ASM in Ghana. *Environ. Chall.* **2021**, *3*, 100053. [CrossRef]
26. Gallwey, J.; Robiati, C.; Coggan, J.; Vogt, D.; Eyre, M. A Sentinel-2 Based Multispectral Convolutional Neural Network for Detecting Artisanal Small-Scale Mining in Ghana: Applying Deep Learning to Shallow Mining. *Remote Sens. Environ.* **2020**, *248*, 111970. [CrossRef]
27. Lymburner, L.; Botha, E.; Hestir, E.; Anstee, J.; Sagar, S.; Dekker, A.; Malthus, T. Landsat 8: Providing Continuity and Increased Precision for Measuring Multi-Decadal Time Series of Total Suspended Matter. *Remote Sens. Environ.* **2016**, *185*, 108–118. [CrossRef]
28. Xing, Q.; Lou, M.; Chen, C.; Shi, P. Using in Situ and Satellite Hyperspectral Data to Estimate the Surface Suspended Sediments Concentrations in the Pearl River Estuary. *IEEE J. Sel. Top. Appl. Earth Obs. Remote Sens.* **2013**, *6*, 731–738. [CrossRef]
29. Forkuor, G.; Ullmann, T.; Griesbeck, M. Mapping and Monitoring Small-Scale Mining Activities in Ghana Using Sentinel-1 Time Series (2015–2019). *Remote Sens.* **2020**, *12*, 911. [CrossRef]
30. Kimijima, S.; Sakakibara, M.; Nagai, M. Characterizing Time-Series Roving Artisanal and Small-Scale Gold Mining Activities in Indonesia Using Sentinel-1 Data. *Int. J. Environ. Res. Public Health* **2022**, *19*, 6266. [CrossRef]
31. Gilvear, D.J.; Waters, T.M.; Milner, A.M. Image analysis of aerial photography to quantify changes in channel morphology and instream habitat following placer mining in interior Alaska. *Freshw. Biol.* **1995**, *34*, 389–398. [CrossRef]
32. Park, S.; Choi, Y. Applications of Unmanned Aerial Vehicles in Mining from Exploration to Reclamation: A Review. *Minerals* **2020**, *10*, 663. [CrossRef]
33. Ren, H.; Zhao, Y.; Xiao, W.; Hu, Z. A review of UAV monitoring in mining areas: Current status and future perspectives. *Int. J. Coal. Sci. Technol.* **2019**, *6*, 320–333. [CrossRef]
34. Padró, J.C.; Carabassa, V.; Balagué, J.; Brotons, L.; Alcañiz, J.M.; Pons, X. Monitoring opencast mine restorations using Unmanned Aerial System (UAS) imagery. *Sci. Total Environ.* **2019**, *657*, 1602–1614. [CrossRef]
35. Jackisch, R.; Lorenz, S.; Zimmermann, R.; Möckel, R.; Gloaguen, R. Drone-borne hyperspectral monitoring of acid mine drainage: An example from the Sokolov Lignite District. *Remote Sens.* **2018**, *10*, 385. [CrossRef]
36. Egidarev, E.G.; Simonov, E.A. Assessment of the Environmental Effect of Placer Gold Mining in the Amur River Basin. *Water Resour.* **2015**, *42*, 897–908. [CrossRef]
37. Khristov, V.K. *History Pages. 80 Years of Susuman GOK. 65 Years of Susumansky District*; Okhotnik publisher: Magadan, Russia, 2018; 280p. (In Russian)
38. Gold Mining in the Magadan Region. Available online: https://zolotodb.ru/article/11259/?page=all (accessed on 30 June 2023). (In Russian)
39. Ilyushina, P.G.; Shikhov, A.N.; Makarieva, O.M. Satellite-Based Mapping of the Negative Impact of Gold Mining Enterprises on the Natural Environment of the Cryolithozone (On the Example of the Magadan Region). *Issled. Zemli Iz Kosmosa* **2023**, *1*, 41–52.
40. Grandmont, K.; Roy, L.-P.; de Grandpré, I.; Fortier, D.; Benkert, B.; Lewkowicz, A. Impact of land cover disturbance on permafrost landscapes. In case studies from Yukon communities. In Proceedings of the GeoQuebec 2015—7th Canadian Permafrost Conf. and 68th Canadian Geotechnical Conference, Quebec City, QC, Canada, 20–23 September 2015; p. 8. [CrossRef]
41. Zarovnyaev, B.; Shubin, G.; Sobakina, M.; Budikina, M. Development of environmentally safe mining technologies taking into account thermomechanical conditions of the permafrost zone. *IOP Conf. Series Earth Environ. Sci.* **2019**, *221*, 012118. [CrossRef]
42. Kornienko, S.G. Characteristics of anthropogenic transformations of landscapes in the area of Bovanenkovo gas field based on Landsat satellite data. *Sovrem. Probl. Distantsionnogo Zondirovaniya Zemli Iz Kosmosa* **2022**, *19*, 106–129. [CrossRef]
43. Tikhmenev, P.E.; Smirnov, A.A.; Tikhmenev, E.A.; Stanchenko, G.V. Anthropogenic dynamics and recovery of disturbed landscapes at the Far East Russia permafrost area. *E3S Web Conf.* **2020**, *169*, 3009. [CrossRef]
44. Rosnedra. Federal Agency for Subsoil Use. Available online: https://www.rosnedra.gov.ru/ (accessed on 15 May 2023).
45. Makarieva, O.; Nesterova, N.; Shikhov, A.; Zemlianskova, A.; Luo, D.; Ostashov, A.; Alexeev, V. Giant Aufeis—Unknown Glaciation in North-Eastern Eurasia According to Landsat Images 2013–2019. *Remote Sens.* **2022**, *14*, 4248. [CrossRef]
46. Zveryaev, I.I.; Arkhipkin, A.V. Variability and Changes of the Growing Season Length and Frost Days Number in Russian sub-Arctic. *Geogr. Environ. Sustain.* **2019**, *12*, 13–22. [CrossRef]
47. Kovalskyy, V.; Roy, D.P. The global availability of Landsat 5 TM and Landsat 7 ETM+ land surface observations and implications for global 30m Landsat data product generation. *Remote Sens. Environ.* **2013**, *130*, 280–293. [CrossRef]
48. Masek, J.G.; Vermote, E.F.; Saleous, N.E.; Wolfe, R.; Hall, F.G.; Huemmrich, K.F.; Gao, F.; Kutler, J.; Lim, T.-K. A Landsat surface reflectance dataset for North America, 1990–2000. *IEEE Geosci. Remote Sens. Lett.* **2006**, *3*, 68–72. [CrossRef]

49. Main-Knorn, M.; Pflug, B.; Louis, J.; Debaecker, V.; Müller-Wilm, U.; Gascon, F. Sen2Cor for Sentinel-2. In Proceedings of the SPIE Remote Sensing, Warsaw, Poland, 11–12 September 2017; Volume 10427, p. 1042704. [CrossRef]
50. USGS EarthExplorer. Available online: https://earthexplorer.usgs.gov/ (accessed on 15 May 2023).
51. EOS LandViewer. Available online: https://eos.com/landviewer (accessed on 15 May 2023).
52. ALOS Global Digital Surface Model "ALOS World 3D—30m (AW3D30)". Available online: https://www.eorc.jaxa.jp/ALOS/en/dataset/aw3d30/aw3d30_e.htm (accessed on 15 May 2023).
53. Fire Information for Resource Management System. Available online: https://www.earthdata.nasa.gov/learn/find-data/near-real-time/firms/active-fire-data (accessed on 15 May 2023).
54. Arino, O.; Bicheron, P.; Achard, F.; Latham, J.; Witt, R.; Weber, J.-L. GlobCover: The most detailed portrait of Earth. *Eur. Space Agency Bull.* **2008**, *136*, 24–31.
55. Bartalev, S.A.; Egorov, V.A.; Zharko, V.O.; Lupyan, E.A.; Plotnikov, D.E.; Khvostikov, S.A.; Shabanov, N.V. *Satellite-Based Mapping of the Vegetation Cover of Russia*; Institute of Space Research of RAS: Moscow, Russia, 2016; Volume 208. (In Russian)
56. Ngom, N.M.; Mbaye, M.; Baratoux, D.; Baratoux, L.; Catry, T.; Dessay, N.; Faye, G.; Sow, E.H.; Delaitre, E. Mapping artisanal and small-scale gold mining in Senegal using Sentinel 2 data. *GeoHealth* **2020**, *4*, e2020GH000310. [CrossRef] [PubMed]
57. Xu, H. Modification of normalized difference water index (NDWI) to enhance open water features in remotely sensed imagery. *Int. J. Remote Sens.* **2006**, *27*, 3025–3033. [CrossRef]
58. Wilson, J.P.; Gallant, J.C. *Terrain Analysis—Principles and Applications*; John Wiley: New York, NY, USA, 2000.
59. Gao, B.-C. NDWI—A normalized difference water index for remote sensing of vegetation liquid water from space. *Remote Sens. Environ.* **1996**, *58*, 257–266. [CrossRef]
60. Belikovich, A.V. *Vegetation Cover of the Susuman District of the Magadan Region. Komarovsky Readings*; Dal'nauka: Vladivostok, Russia, 2001; Volume 48, pp. 125–154. (In Russian)
61. Gorelick, N.; Hancher, M.; Dixon, M.; Ilyushchenko, S.; Thau, D.; Moore, R. Google Earth Engine: Planetary-scale geospatial analysis for everyone. *Remote Sens. Environ.* **2017**, *202*, 18–27. [CrossRef]
62. Breiman, L.; Friedman, J.H.; Olshen, R.A.; Stone, C.J. *Classification and Regression Trees*; Wadsworth Inc.: Middleburg Heights, OH, USA, 1984.
63. Konstantinov, M.M. *Gold Mining Provinces of the World*; Nauchnyy mir: Moscow, Russia, 2006; 358p. (In Russian)
64. *State Report on the State and Use of Mineral Resources of the Russian Federation in 2020*; Ministry of Natural Resources and Environment of the Russian Federation: Moscow, Russia, 2021; 572p. (In Russian)
65. Chupachenko, O.N. *Educational and Methodological Manual for Public Monitoring of River Pollution during the Extraction of Alluvial Gold Using Satellite Images*; World Wildlife Fund (WWF): Moscow, Russia, 2020; 36p. (In Russian)
66. Egidarev, E. Map of Satellite Monitoring of Alluvial Gold Mining in Siberia and the Far East. Available online: https://zolotari.net/map (accessed on 30 June 2023). (In Russian)
67. Simonov, E.A. *Golden Rivers: Issue 1. Amur Basin*; World Wildlife Fund (WWF): Vladivostok, Russia, 2012; 120p. (In Russian)
68. Yaborov, V.T. Restoration of vegetation cover on man-made landscapes of allower gold mining in the Amur region. *Far East. Agrar. Bull.* **2008**, *1*, 86–92. (In Russian)
69. Tsydypova, M.V.; Suprunenko, A.G. GIS mapping of anthropogenic impact on the environment by the extraction of placer gold (on the example of Eravninsky district of the Republic of Buriatia). *Bull. Sib. State Univ. Geosyst. Tech.* **2017**, *22*, 119–127. (In Russian)
70. Yu, L.; Xu, Y.; Xue, Y.; Li, X.; Cheng, Y.; Liu, X.; Porwal, A.; Holden, E.-J.; Yang, J.; Gong, P. Monitoring surface mining belts using multiple remote sensing datasets. *Ore Geol. Rev.* **2018**, *101*, 675–687. [CrossRef]